

Identification of the type of stent with three-dimensional optical coherence tomography: the SPQR study

Carlos Cortés^{1,2}, MD, PhD; Miao Chu^{3,4}, MS; Michele Schincariol⁵, MD; Miguel Ángel Martínez-Hervás-Alonso³, MD; Bernd Reisbeck³, MD; Ruiyan Zhang^{6,7}, MD, PhD; Yoshinobu Murasato⁸, MD, PhD; Shao-Liang Chen⁹, MD, PhD; Francesco Lavarra¹⁰, MD; Shengxian Tu⁴, PhD; Sigmund Silber¹¹, MD, FESC, FACC; Juan Luis Gutiérrez-Chico^{1,3,12*}, MD, PhD, FESC, FACC

1. Klinikum Frankfurt (Oder), Frankfurt, Germany; 2. San Pedro Hospital, Logroño, Spain; 3. Cardiology Department, Campo de Gibraltar Health Trust, Algeciras, Spain; 4. Med-X Research Institute, School of Biomedical Engineering, Shanghai Jiao Tong University, Shanghai, China; 5. Klinikum Fürth, Fürth, Germany; 6. Ruijin Hospital, Shanghai, China; 7. Medical University, Shanghai Jiao Tong University, Shanghai, China; 8. Kyushu Medical Center, Fukuoka, Japan; 9. Nanjing First Hospital, Nanjing, China; 10. Jilin Heart Hospital, Changchun, China; 11. Cardiology Practice, Munich, Germany; 12. DRK Klinikum Westend, Berlin, Germany

C. Cortés and M. Chu contributed equally to this manuscript.

This paper also includes supplementary data published online at: <https://eurointervention.pcronline.com/doi/10.4244/EIJ-D-20-00598>

KEYWORDS

- bare metal stent
- bioresorbable scaffolds
- drug-eluting stent
- optical coherence tomography

Abstract

Background: The ability of optical coherence tomography (OCT) to identify specific types of stent has never been systematically studied.

Aims: The aim of this study was to test the accuracy of OCT imaging to identify patterns of stent platform and subsequently identify the type of stent implanted.

Methods: Consecutive patients from six international centres were retrospectively screened, searching for OCT studies with metallic stents or scaffolds. The sample was analysed by two blinded operators, applying a dedicated protocol in four steps to identify the type of stent: 1) 3D and automatic strut detection (ASD), 2) 3D tissue view, 3) longitudinal view with ASD, 4) mode “stent only” and ASD.

Results: A series of 212 patients underwent OCT in the study centres, finding 294 metallic stents or scaffolds in 146 patients. The protocol correctly identified 285 stents (96.9%, kappa 0.965), with excellent interobserver agreement (kappa 0.988). The performance tended to be better in recently implanted stents (kappa 0.993) than in stents implanted ≥ 3 months before (kappa 0.915), and in pullback speed 18 mm/s as compared with 36 mm/s (kappa 0.969 vs 0.940, respectively).

Conclusions: The type of stent platform can be accurately identified in OCT by trained analysts following a dedicated protocol, combining 3D-OCT, ASD and longitudinal view. This might be clinically helpful in scenarios of device failure and for the quantification of apposition. The blinding of analysts in OCT studies should be revisited.

*Corresponding author: Department of Cardiology, Hospital Punta de Europa, Crtra. Getares s/n, 11207 Algeciras (Cádiz), Spain. E-mail: juanluis.gutierrezchico@ictra.es

Abbreviations

| | |
|---------------|--|
| ASD | automatic strut detection |
| BRS | bioresorbable scaffold |
| DES | drug-eluting stent |
| ISR | in-stent restenosis |
| LAD | left anterior descending |
| NIR | near-infrared |
| NURD | non-uniform rotational distortion |
| OCT | optical coherence tomography |
| RCA | right coronary artery |
| 3D-OCT | three-dimensional optical coherence tomography |

Introduction

Three-dimensional (3D) optical coherence tomography (OCT) has proven its usefulness for the treatment of complex bifurcations, to assist the wire recrossing through the right stent cell¹ or to assess the structural integrity of bioresorbable scaffolds (BRS)^{2,3}. The ability of 3D-OCT to identify the type of stent implanted, in case this information was unknown and relevant, has been suggested in some reports⁴, but its accuracy for this indication has never been systematically studied. The identification of the stent is clinically and scientifically relevant, because it might provide the operator with meaningful information to make tailored decisions in challenging cases, particularly in the setting of device failure^{4,5}, and also for accurate quantification of apposition^{6,7}, or because it might jeopardise the blinding of the analysts in randomised clinical trials involving OCT quantification⁶⁻⁸.

The Stent Pattern Qualitative Recognition (SPQR) study appraises the feasibility and accuracy of identifying the type of stent previously implanted by means of 3D-OCT, strut automatic detection and longitudinal OCT reconstruction.

Editorial, see page 103

Methods

Consecutive patients undergoing OCT of a coronary artery previously treated with implantation of a metallic stent, durable or bioresorbable, in any of the participating centres (Klinikum Frankfurt Oder, Germany; DRK Klinikum Westend, Berlin, Germany, and Campo de Gibraltar Health Trust, Algeciras, Spain) between March 2016 and August 2019 were retrospectively included in the study. Exclusion criteria were 1) previous treatment of the target vessel with non-metallic bioresorbable scaffolds alone; 2) overlapping stents or multiple stent layers leaving a <5 mm monolayer segment; 3) poor OCT quality due to non-uniform rotational distortion (NURD), incomplete purge of the optical catheter, suboptimal vessel flushing or other artefacts⁹, and 4) severe stent distortion due to longitudinal stress or collapse of the lumen, leaving <5 mm of stent structurally preserved and suitable for analysis. All OCT studies were acquired with a Dragonfly™ catheter and an ILUMIEN™ OPTIS™ system (Abbott, St. Paul, MN, USA), at a rotation speed of 180 Hz and a pullback speed of 18 mm/s or 36 mm/s, resulting in longitudinal resolutions of 0.1 and 0.2 mm, respectively. The operators used a non-occlusive technique¹⁰ and automatic contrast injection, calculating

the contrast volume with a formula to optimise quality with a minimal amount of dye¹¹. The sample was completed with selected cases from three Asian centres, containing paradigmatic examples of some stent types not found in the European sample. These selected cases were intercalated into the sample at random positions for analysis.

Clinical information about patients, procedures and types of stent previously implanted was retrospectively collected from clinical recordings in each centre. Target stents were classified as recently (<3 months) or late implanted (≥3 months).

The study complied with the principles of good clinical practice and with the Declaration of Helsinki for investigation in human beings. The study protocol was approved by the institutional review boards of the participating hospitals.

NOMENCLATURE FOR DESCRIPTION OF THE STENT PLATFORMS

Although most technical studies describe the stent platforms in terms of peaks or valleys depending on the angle between the longitudinal connector and the hoops (obtuse or acute, respectively)¹²⁻¹⁴, this terminology proved to be inappropriate for the current analysis, because it created unsolvable ambiguities. A specifically dedicated nomenclature was defined.

Two fundamental components were considered - sinusoidal hoops and longitudinal connectors. Peaks and valleys were defined in the sinusoidal hoops as hinge points with the vertex pointing to the distal and proximal parts of the vessel, respectively (**Figure 1**). The struts connecting peaks and valleys were dubbed slopes. Hoops were considered in-phase if peaks faced peaks in adjacent hoops, out-of-phase if peaks faced valleys, or offset if peaks faced slopes. Longitudinal connectors were defined according to the points of the hoop that they connected (peak-to-peak, peak-to-valley, valley-to-valley or connecting the slopes) (**Figure 2**), and according to unique morphological features of their design (crenelated, S-shaped, step-shaped, etc.).

PATTERNS OF THE DIFFERENT STENT PLATFORMS AND OCT ANALYSIS

The characteristics of the stent platforms in this study, according to the nomenclature explained above, are summarised in **Supplementary Table 1** and **Figure 3**.

OCT raw data were evaluated by two independent blinded analysts, using an ILUMIEN OPTIS E.5 workstation (Abbott). After identification of the stented segment and the corresponding analysable monolayer (in case of overlapping), the analysts undertook the following protocol to identify the pattern of the stent platform, rotating the image at their discretion: 1) 3D view with automatic strut detection (ASD); 2) 3D tissue view, without ASD; 3) longitudinal view with ASD; and 4) 3D view in mode “stent only” (**Figure 4**). The analysts recorded at which steps of the protocol the type of stent platform could be recognised. After completing the four steps of the protocol, the analyst had to identify the type of stent previously implanted as one of the 20 categories defined in **Supplementary Table 1** and **Figure 3** or label the case as unrecognisable.

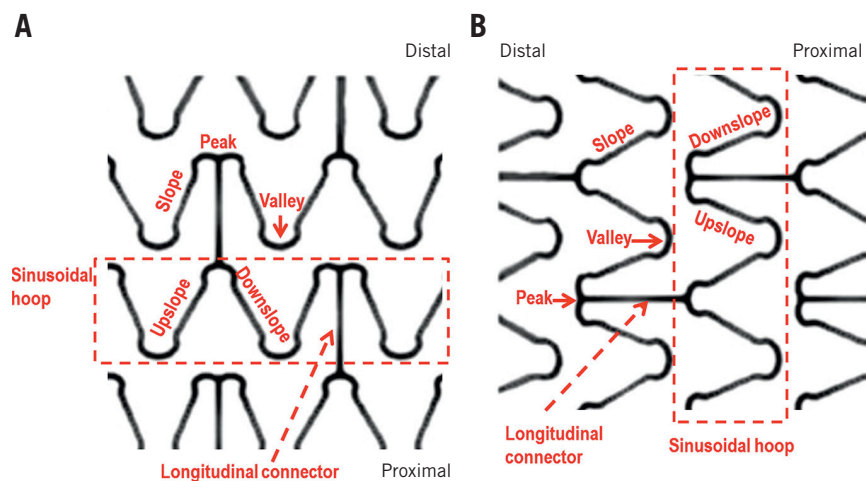


Figure 1. Nomenclature of the stent platform for the current study. The two fundamental components were sinusoidal hoops and the longitudinal connectors. Peaks and valleys were defined in the hoops as if the proximal part of the vessel were the earth and the distal part were the sky (A). Hinge points with the vertex pointing to the distal part were peaks, while hinge points with the vertex pointing to the proximal part were valleys. The struts between peaks and valleys were dubbed slopes. The terms upslope and downslope were defined according to a consistent direction (for instance left to right) at the analyst's discretion. B) OCT view, with the distal part at the left part of the screen.

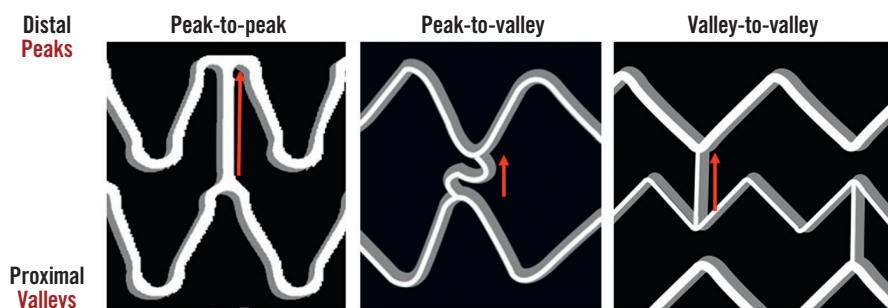


Figure 2. Nomenclature of longitudinal connectors for the current study. Longitudinal connectors (or direct connections) peak-to-peak, peak-to-valley and valley-to-valley.

STATISTICAL ANALYSIS

Descriptive statistics of continuous variables were reported as mean±SD if they followed a Gaussian distribution or as median (quartiles) if differently distributed, while those of categorical variables were presented as counts (percentages). The agreement between analyst 1 and the type of stent platform previously implanted was reported as kappa coefficient and stratified according to the timing of stent implant (recently vs late implanted) and pullback speed (18 vs 36 mm/s). Interobserver reproducibility was reported as kappa coefficient. Efficiency analysis of the steps was reported as % of stents recognised in each step. All analyses were performed with SPSS, Version 24.0 software package (IBM Corp., Armonk, NY, USA).

Results

A total of 193 patients underwent OCT studies in the enrolling centres during the study period. The sample was completed with 19 selected patients from Asian centres with paradigmatic

examples of specific stent types. Sixty-six patients (68 studies) were excluded: 40 because no stent was imaged in the OCT study (58.8%), 22 because only non-metallic BRS were implanted in the intervention (32.4%), 3 due to suboptimal vessel flushing (4.4%), 2 due to severe stent distortion (2.9%), and 1 due to NURD (1.5%). During the analysis 21 stents were excluded due to multi-layer (8), overlap with <5 mm of monolayer (8), suboptimal vessel flushing (3), incomplete purge of the optical catheter (1) or NURD (1). A total of 146 patients, 155 procedures, 179 lesions, 196 pullbacks and 294 stents were finally analysed according to the protocol (Figure 5).

DESCRIPTIVE STATISTICS OF THE SAMPLE

Table 1 and Table 2 present the descriptive statistics of the sample. Different types of stent were analysed in the study: MULTI-LINK RX PIXEL™, MULTI-LINK ZETA, MULTI-LINK VISION® and XIENCE (Abbott Vascular, Santa Clara, CA, USA); Driver®, Resolute Integrity® and Resolute Onyx™ (Medtronic, Santa

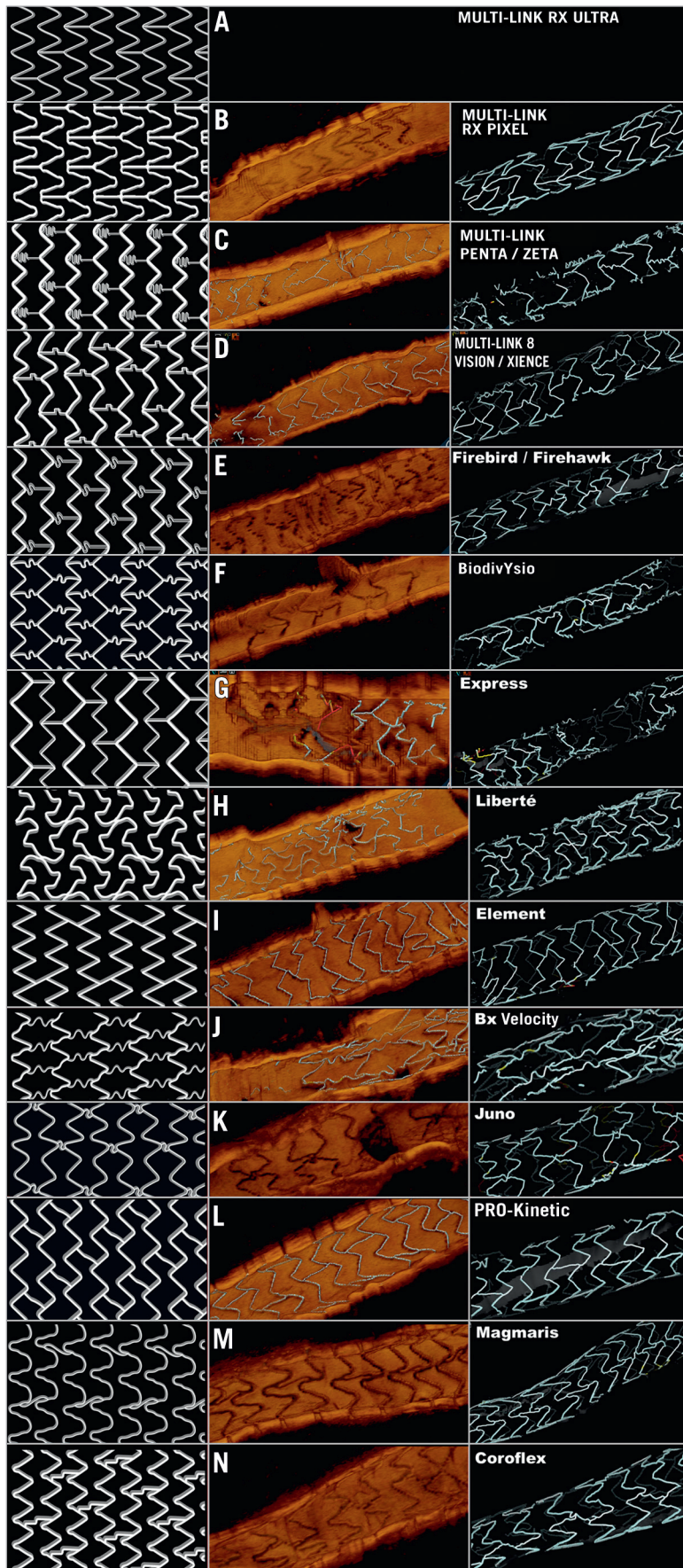


Figure 3. Design and OCT examples of the different stent platforms in the study.

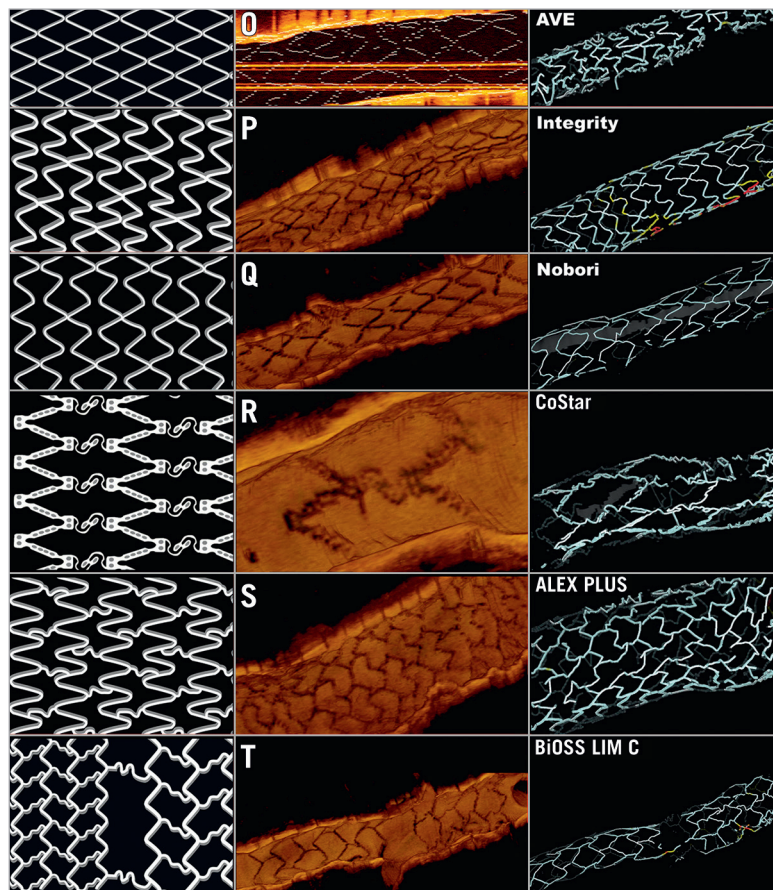


Figure 3 (continued). Design and OCT examples of the different stent platforms in the study.

Rosa, CA, USA); Orsiro and Magmaris® (Biotronik AG, Bülach, Switzerland); BioMatrix™ and BioFreedom™ (Biosensors, Morges, Switzerland); Coroflex® (B. Braun, Melsungen, Germany); CYPHER Select® (Cordis, Cardinal Health, Milpitas,

CA, USA); TAXUS Express, TAXUS Liberté™ and PROMUS Element™ (Boston Scientific, Marlborough, MA, USA); Nobori® (Terumo, Tokyo, Japan); Firebird™ and Firehawk® (MicroPort, Shanghai, China); ALEX® PLUS and BiOSS LIM C (Balton,

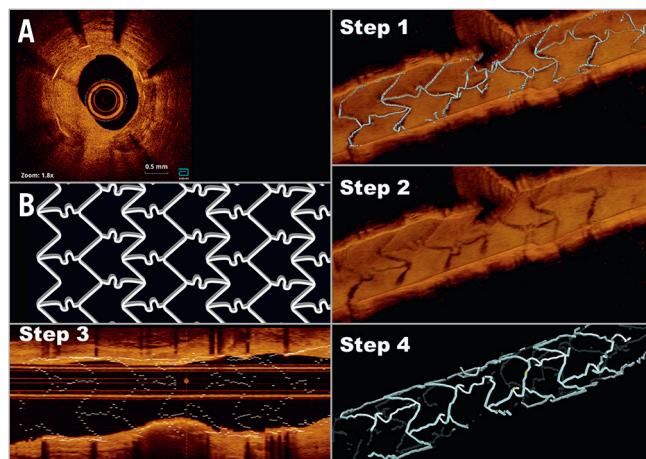


Figure 4. Paradigmatic case of a restenosis (A) in a BiodivYsio stent (B), showing the four steps of the protocol. Step 1: 3D view with automatic detection of struts. Step 2: 3D direct tissue view, without automatic detection of struts. Step 3: longitudinal view with automatic detection of struts. Step 4: 3D view in “stent only” mode.

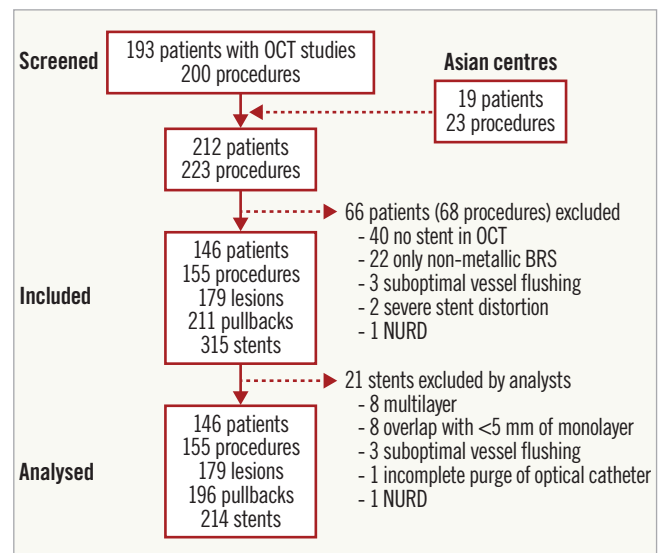


Figure 5. Study flow chart. NURD: non-uniform rotational distortion; OCT: optical coherence tomography

Table 1. Descriptive statistics of patients, interventions and lesions.

| Patient level | | n=146 | |
|---|-------------------------|--------------------------|-----------|
| Male (%) | | 112 (76.7) | |
| Age, years | | 66.0 (59.0-75.2) | |
| BMI (SD) | | 28.1 (4.8) | |
| CV risk factors | Hypertension | 118 (80.8) | |
| | Hypercholesterolaemia | 70 (47.9) | |
| | Diabetes mellitus | Type 2 on OAD | 41 (28.1) |
| | | Type 2 insulin-requiring | 12 (8.2) |
| | Smoking | Previous smoker | 28 (19.2) |
| Current smoker | | 34 (23.3) | |
| Family history of CHD | | 7 (4.8) | |
| Previous MI | | 54 (37.0) | |
| Previous revascularisation | PCI | 81 (55.5) | |
| | CABG | 9 (6.2) | |
| GFR (Cockcroft-Gault), ml/min | | 86.8 (45.3) | |
| Serum haemoglobin, g/dl | | 13.5 (1.7) | |
| LVEF, % | | 60 (12) | |
| Procedural variables | | n=155 | |
| SYNTAX score | | 13.7 (8.6) | |
| Contrast volume, ml | | 232 (106) | |
| Fluoroscopy time, min | | 20.8 (15.8) | |
| Clinical indication | Stable coronary disease | 108 (69.7) | |
| | Unstable angina | 22 (14.2) | |
| | Non-ST-elevation MI | 22 (14.2) | |
| | ST-elevation MI | 3 (1.9) | |
| Lesions | | n=179 | |
| Calcification | None to little | 155 (86.6) | |
| | Moderate to severe | 24 (13.4) | |
| DS, % | | 72.5 (15.9) | |
| Data presented as counts (percent), mean (standard deviation) or median (P25-P75). BMI: body mass index; CABG: coronary artery bypass graft; CHD: coronary heart disease; CV: cardiovascular; DS: diameter stenosis; GFR: glomerular filtration rate; LVEF: left ventricular ejection fraction; MI: myocardial infarction; OAD: oral antidiabetics; PCI: percutaneous coronary intervention | | | |

Warsaw, Poland); BiodivYsio (Biocompatibles Ltd, Farnham, United Kingdom), and CoStar™ (Conor Medsystems, Menlo Park, CA, USA)¹⁵. One hundred and seven stents (36.4%) were implanted more than three months prior to the OCT study and 62 (21.1%) presented in-stent restenosis (ISR) as an anatomic substrate for the clinical symptoms. All but three of the ISR stents were implanted ≥ 3 months before. Most studies (77.2%) were acquired at a pullback speed of 18 mm/s.

FEASIBILITY, AGREEMENT AND REPRODUCIBILITY

Eight cases (2.7%) were deemed unrecognisable by the main analyst and in one additional case (0.3%) the identification was wrong. Five unrecognisable cases and the misclassified stent corresponded to ISR. All other cases were correctly identified, resulting

Table 2. Descriptive statistics of the analysed stents.

| Stents analysed | | n=294 |
|--|-----------------------------------|-----------------|
| Coronary artery | Left main | 11 (3.7) |
| | Left anterior descending | 123 (41.8) |
| | Diagonal | 12 (4.1) |
| | Circumflex | 45 (15.3) |
| | Obtuse marginal | 10 (3.4) |
| | Right coronary artery | 91 (31.0) |
| | Posterolateral | 2 (0.7) |
| Type of stent implanted | XIENCE | 69 (23.5) |
| | Magmaris | 55 (18.7) |
| | BioFreedom | 23 (7.8) |
| | Firebird | 22 (7.5) |
| | Resolute Integrity | 19 (6.5) |
| | Orsiro | 17 (5.8) |
| | Coroflex | 14 (4.8) |
| | PROMUS Element | 12 (4.1) |
| | BIOSS-LIM C | 10 (3.4) |
| | MULTI-LINK RX PIXEL | 9 (3.1) |
| | Firehawk | 9 (3.1) |
| | Resolute Onyx | 7 (2.4) |
| | Driver | 6 (2.0) |
| | TAXUS Liberté | 4 (1.4) |
| | Nobori | 4 (1.4) |
| | BioMatrix | 3 (1.0) |
| | MULTI-LINK ZETA | 2 (0.7) |
| | VISION | 2 (0.7) |
| | BiodivYsio | 2 (0.7) |
| | ALEX PLUS | 2 (0.7) |
| | CYPHER | 1 (0.3) |
| | TAXUS Express | 1 (0.3) |
| | CoStar | 1 (0.3) |
| Timing of implant | Recently implanted (<3 months) | 187 (63.6) |
| | Late implanted (≥ 3 months) | 107 (36.4) |
| Immediately post implant | | 160 (54.4) |
| Time from stent implantation, months * | | 23.9 (8.7-61.6) |
| In-stent restenosis | | 62 (21.1) |
| Mehran type [§] | Ia | 1 (1.6) |
| | Ib | 3 (4.8) |
| | Ic | 11 (17.7) |
| | Id | 0 (0.0) |
| | II | 27 (43.6) |
| | III | 18 (29.0) |
| | IV | 2 (3.2) |
| Overlap | | 132 (44.9) |
| Pullback speed | 18 mm/s | 227 (77.2) |
| | 36 mm/s | 67 (22.8) |
| Data presented as counts (percent) or median (P25-P75). * For the group of late implanted stents. [§] For the subgroup with in-stent restenosis. LVEF: left ventricular ejection fraction | | |

in a feasibility of 96.9%, kappa 0.965 (95% CI: 0.943–0.987; $p < 0.0001$). Both analysts agreed in all but three cases (1.0%), corresponding to a kappa 0.988 (95% CI: 0.974–1.00, $p < 0.0001$) for the interobserver agreement (Table 3).

Table 3 presents the results of agreement stratified by timing of stent implant and by pullback speed. The agreement tended to be worse in late implanted stents (kappa 0.915; 95% CI: 0.860–0.970), in cases of ISR (kappa 0.889; 95% CI: 0.807–0.971) and if the pullback was acquired at 36 mm/s (kappa 0.940; 95% CI: 0.875–1.000). Conversely, recently implanted stents were accurately identified in all but one case, thus presenting a kappa coefficient close to perfect agreement (kappa 0.993; 95% CI: 0.981–1.000).

Table 3. Agreement between the stent platform identified by the analysts and the platform implanted.

| | Kappa | 95% CI | | p-value |
|---|---------------|--------|-------|---------|
| | | Lower | Upper | |
| Agreement with implanted stent platform | 0.965 | 0.943 | 0.987 | <0.0001 |
| Recently implanted (<3 months) | 0.993 (0.006) | 0.981 | 1.000 | <0.0001 |
| Late implanted (≥ 3 months) | 0.915 (0.028) | 0.860 | 0.970 | <0.0001 |
| ISR | 0.889 (0.042) | 0.807 | 0.971 | <0.0001 |
| PB speed 18 mm/s | 0.969 (0.013) | 0.944 | 0.994 | <0.0001 |
| PB speed 36 mm/s | 0.940 (0.033) | 0.875 | 1.000 | <0.0001 |
| Interobserver agreement | 0.988 | 0.974 | 1.000 | <0.0001 |

CI: confidence interval; ISR: in-stent restenosis; PB: pullback

EFFICIENCY OF THE PROTOCOL STEPS

In recently implanted stents, step 2 (3D tissue view) was the most effective (100% identification at 18 mm/s; 97.7% at 36 mm/s) (Table 4, Figure 6). In 14 cases (7.5%), the stent could be recognised only in step 2 (Table 4, Figure 7).

Conversely, in late implanted stents the most efficient step was step 3 (longitudinal view) - 90.4% identification at 18 mm/s; 91.7% at 36 mm/s (Table 4, Figure 6). The combination of steps played a critical role in late implanted stents, as 5 cases (4.7%) were only identifiable in step 3 and 3 cases (2.8%) only identifiable in step 2 (Table 4, Figure 7).

Discussion

The current study proves that the type of stent previously implanted in a coronary artery can be accurately identified by OCT, combining 3D reconstruction, ASD and longitudinal view. An operative description of the different stent platforms, based on simple differential features of their design, together with a systematic stepwise protocol, resulted in accurate pattern recognition by trained analysts, with excellent feasibility and reproducibility.

The identification of the specific type of stent implanted might be important in different clinical scenarios, mostly related to stent failure, as patients often undergo the intervention before all

Table 4. Efficiency of each step to recognise the stent.

| | Recently implanted | Late implanted |
|---------------------------------|--------------------|----------------|
| PB speed 18 mm/s | 144 | 83 |
| Step 1: 3D with automatic strut | 127 (88.2) | 70 (84.3) |
| Step 2: 3D tissue | 144 (100.0) | 65 (78.3) |
| Step 3: longitudinal view | 131 (91.0) | 75 (90.4) |
| Step 4: 3D stent only | 127 (88.2) | 66 (79.5) |
| PB speed 36 mm/s | 43 | 24 |
| Step 1: 3D with automatic strut | 32 (74.4) | 16 (66.7) |
| Step 2: 3D tissue | 42 (97.7) | 14 (58.3) |
| Step 3: longitudinal view | 41 (95.3) | 22 (91.7) |
| Step 4: 3D stent only | 32 (74.4) | 14 (58.3) |
| Step 1 | 159 (85.0) | 86 (80.4) |
| Step 2 | 186 (99.5) | 79 (73.8) |
| Step 3 | 172 (92.0) | 97 (90.7) |
| Step 4 | 159 (85.0) | 80 (74.8) |
| Combination of steps | 187 | 107 |
| Unrecognisable | 1 (0.5) | 7 (6.5) |
| Step 1 only | 0 (0.0) | 0 (0.0) |
| Step 2 only | 14 (7.5) | 3 (2.8) |
| Step 3 only | 0 (0.0) | 5 (4.7) |
| Step 4 only | 0 (0.0) | 0 (0.0) |
| Steps 1+2 | 0 (0.0) | 0 (0.0) |
| Steps 1+3 | 0 (0.0) | 2 (1.9) |
| Steps 1+4 | 0 (0.0) | 0 (0.0) |
| Steps 2+3 | 13 (7.0) | 5 (4.7) |
| Steps 2+4 | 0 (0.0) | 0 (0.0) |
| Steps 3+4 | 0 (0.0) | 0 (0.0) |
| Steps 1+2+3 | 0 (0.0) | 5 (4.7) |
| Steps 1+2+4 | 0 (0.0) | 0 (0.0) |
| Steps 1+3+4 | 0 (0.0) | 14 (13.1) |
| Steps 2+3+4 | 0 (0.0) | 1 (0.9) |
| All the steps | 159 (85.0) | 65 (60.7) |

Data presented as count (percent) of stents that were correctly identified. PB: pullback

the relevant information about previous procedures can be reliably collected. As different types of stent are associated with different mechanisms of thrombosis, it is critical to understand the pathophysiology underlying each case in order to implement the most appropriate treatment. First-generation drug-eluting stents (DES) were associated with hypersensitivity reactions resulting in inflammation and thrombosis^{16,17}, while second-generation DES were not. In a recently published case of very late DES thrombosis, 3D-OCT enabled the identification of a first-generation DES and a second-generation DES in the same vessel: the thrombosis was dependent on the latter due to severe structural distortion⁴. The treatment could then be directed to the restoration of normal biomechanics, with no concerns about implanting more metal or

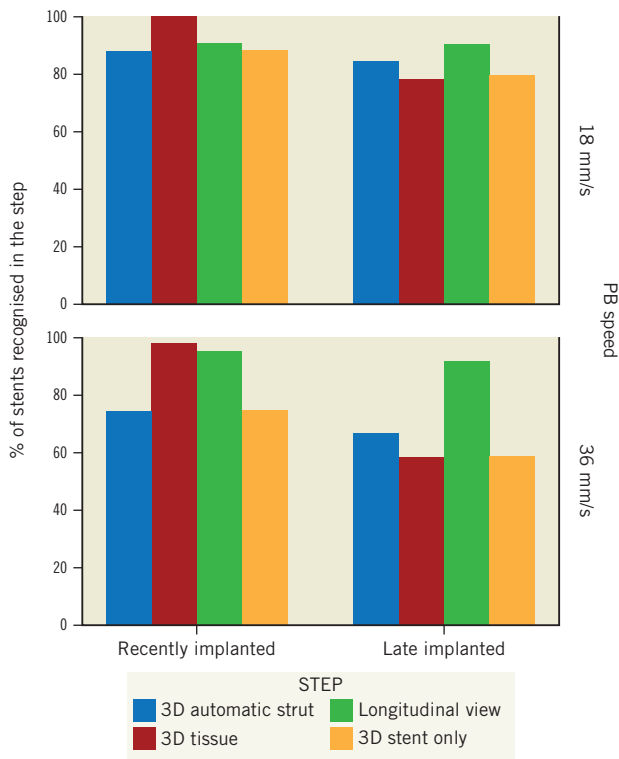


Figure 6. Diagnostic efficiency of each step of the protocol, stratified by timing of the stent implant and by pullback speed.

polymer. The therapeutic plan would have been different if the thrombosis had been dependent on the first-generation DES⁴. Likewise, the most solid evidence to date about the treatment of in-stent restenosis (ISR) indicates that switching to a different type of DES might be better than insisting on the same DES type⁵.

However, the information about the restenosed DES is sometimes missing, due to incomplete reports or patients treated in another centre. An exigent interventional cardiologist must know which type of stent is being treated and the mechanisms that most likely triggered the stent failure. If this information is missing, it can be elucidated with standard OCT.

The quantification of apposition requires the subtraction of the specific strut thickness from the malapposition distance^{6,7}. This method can be inaccurate if the type of stent is unknown or if it must remain unknown, as in the case of randomised studies. The ability of a trained analyst to identify the type of stent should be considered in clinical trials with OCT endpoints, wherein the analyst must be blind to the stent adjudication. The quantification software should not allow the analyst to obtain 3D or longitudinal views with strut detection, because the type of stent would then be unravelled. Artificial intelligence might automate the process of stent recognition for assessment of malapposition in the near future, as deep convolutional networks are already performing ASD taking the stent pattern into account¹⁸.

Our results highlight the importance of combining the different steps of the protocol, particularly in late implanted stents. **Supplementary Table 2** summarises the characteristics and technical requirements of each step. All steps except 3D tissue view depend on ASD, whilst steps 1 and 4 require post-processing of the detected struts. The most efficient steps are independent of these technical tools. Post-processing may be helpful in filling the gaps between struts, rendering an accurate stent structure, but it can be misleading in complex stent designs. In recently implanted stents, 3D tissue view (i.e., the shear OCT image) is the most efficient step, depending only on the longitudinal resolution of the pullback. Late implanted stents, however, are often deeply buried in neointima and leave no recognisable relief on the intimal surface, so 3D tissue view can be outperformed by longitudinal view, depending on the longitudinal resolution and accurate strut detection.

Limitations

This is a retrospective offline analysis performed on standard real-world OCT pullbacks by trained analysts. The performance of the protocol applied by local operators on-site should be prospectively confirmed.

Some DES share the same stent platform as their corresponding bare metal stents or even as other DES. In these cases, the identification of the platform does not permit inferring the exact type, but it substantially reduces the level of uncertainty. Complementary information about local trends on stent availability might often solve the potential ambiguity.

The sample of stents in the study reflects local practice and availability in the study centres. Some platforms were described, but no paradigmatic example of them could be found. The description of these platforms is however kept in the manuscript for didactic purposes. Likewise, some stent platforms excluded from the description might be commonly used in other centres, requiring local adaptations of the protocol.

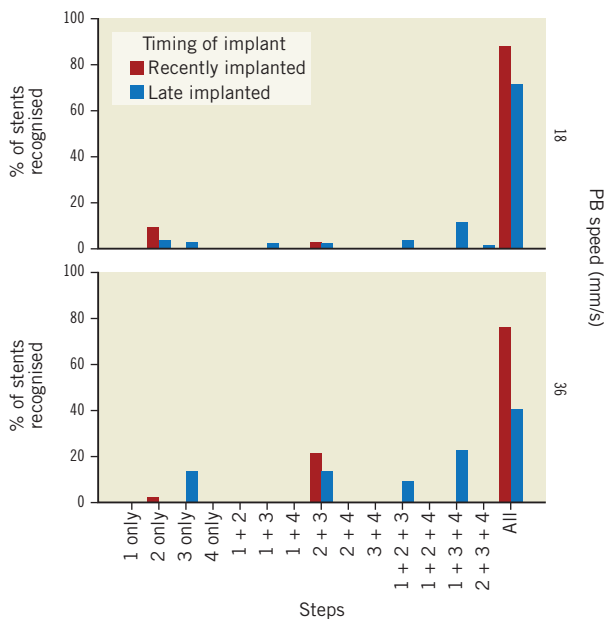


Figure 7. Combination of steps in which the stent is recognised, stratified by timing of the stent implant and by pullback speed.

Conclusions

The stent platform implanted in a coronary artery can be accurately identified in OCT by trained analysts following a dedicated protocol, combining 3D-OCT, automatic strut detection and longitudinal view. This might be clinically helpful in scenarios of device failure and for the quantification of apposition. The blinding of analysts in OCT studies should be revisited.

Impact on daily practice

The ability of OCT to identify the type of stent previously implanted can potentially be useful in cases of stent failure, in which specific information is often missing or misleading at the time of the intervention. The quantification of apposition could be automated and facilitated by incorporating convolutional models for automatic stent identification in future updates of the software. Finally, the blinding of OCT studies must be revisited after proving that a trained analyst can efficiently identify the type of stent aided by 3D reconstruction or by longitudinal view.

Acknowledgements

We wish to thank Lili Liu (Ruijin Hospital, Shanghai), Jing Kan (Nanjing Heart Centre) and Qi Zhou (MicroPort) for their technical assistance.

Conflict of interest statement

The authors have no conflicts of interest to declare.

References

- Okamura T, Nagoshi R, Fujimura T, Murasato Y, Yamawaki M, Ono S, Serikawa T, Hikichi Y, Norita H, Nakao F, Sakamoto T, Shinke T, Shite J. Impact of guidewire recrossing point into stent jailed side branch for optimal kissing balloon dilatation: core lab 3D optical coherence tomography analysis. *EuroIntervention*. 2018;13:e1785-93.
- Gogas BD, van Geuns RJ, Farooq V, Regar E, Heo JH, Ligthart J, Serruys PW. Three-dimensional reconstruction of the post-dilated ABSORB everolimus-eluting bioresorbable vascular scaffold in a true bifurcation lesion for flow restoration. *JACC Cardiovasc Interv*. 2011;4:1149-50.
- Farooq V, Gogas BD, Okamura T, Heo JH, Magro M, Gomez-Lara J, Onuma Y, Radu MD, Brugaletta S, van Bochove G, van Geuns RJ, Garcia-Garcia HM, Serruys PW. Three-dimensional optical frequency domain imaging in conventional percutaneous coronary intervention: the potential for clinical application. *Eur Heart J*. 2013;34:875-85.
- Jaguszewski MJ, Cortes C, Daucher H, Schincariol M, Halejcio M, Besuch P, Gutiérrez-Chico JL. Very late stent thrombosis in everolimus-eluting stent with predisposing mechanical factors: Differential features. *Cardiol J*. 2017;24:345-9.
- Alfonso F, Pérez-Vizcayno MJ, Dutary J, Zueco J, Cequier A, Garcia-Touchard A, Martí V, Lozano I, Angel J, Hernandez JM, Lopez-Minguez JR, Melgares R, Moreno R, Seidelberger B, Fernandez C, Hernandez R; RIBS-III Study Investigators (under the auspices of the Working Group on Interventional Cardiology of the Spanish Society of Cardiology). Implantation of a drug-eluting stent with a different drug (switch strategy) in patients with drug-eluting stent restenosis. Results from a prospective multicenter study (RIBS III [Restenosis Intra-Stent: Balloon Angioplasty Versus Drug-Eluting Stent]). *JACC Cardiovasc Interv*. 2012;5:728-37.
- Gutiérrez-Chico JL, van Geuns RJ, Regar E, van der Giessen WJ, Kelbaek H, Saunamäki K, Escaned J, Gonzalo N, di Mario C, Borgia F, Nuesch E, Garcia-Garcia HM, Silber S, Windecker S, Serruys PW. Tissue coverage of a hydrophilic polymer-coated zotarolimus-eluting stent vs. a fluoropolymer-coated everolimus-eluting stent at 13-month follow-up: an optical coherence tomography substudy from the RESOLUTE All Comers trial. *Eur Heart J*. 2011;32:2454-63.
- Gutiérrez-Chico JL, Regar E, Nüesch E, Okamura T, Wykrzykowska J, di Mario C, Windecker S, van Es GA, Gobbens P, Juni P, Serruys PW. Delayed coverage in

malapposed and side-branch struts with respect to well-apposed struts in drug-eluting stents: in vivo assessment with optical coherence tomography. *Circulation*. 2011;124:612-23.

8. Guagliumi G, Costa MA, Sirbu V, Musumeci G, Bezerra HG, Suzuki N, Matiashvili A, Lortkipanidze N, Mihalesic L, Trivisonno A, Valsecchi O, Mintz GS, Dressler O, Parise H, Maehara A, Cristea E, Lansky AJ, Mehran R, Stone GW. Strut coverage and late malapposition with paclitaxel-eluting stents compared with bare metal stents in acute myocardial infarction: optical coherence tomography substudy of the Harmonizing Outcomes with Revascularization and Stents in Acute Myocardial Infarction (HORIZONS-AMI) Trial. *Circulation*. 2011;123:274-81.

9. Tearney GJ, Regar E, Akasaka T, Adriaenssens T, Barlis P, Bezerra HG, Bouma B, Bruining N, Cho JM, Chowdhary S, Costa MA, de Silva R, Dijkstra J, Di Mario C, Dudek D, Falk E, Feldman MD, Fitzgerald P, Garcia H, Gonzalo N, Granada JF, Guagliumi G, Holm NR, Honda Y, Ikeno F, Kawasaki M, Kochman J, Koltowski L, Kubo T, Kume T, Kyono H, Lam CC, Lamouche G, Lee DP, Leon MB, Maehara A, Manfrini O, Mintz GS, Mizuno K, Morel MA, Nadkarni S, Okura H, Otake H, Pietrasik A, Prati F, Raber L, Radu MD, Rieber J, Riga M, Rollins A, Rosenberg M, Sirbu V, Serruys PW, Shimada K, Shinke T, Shite J, Siegel E, Sonada S, Suter M, Takarada S, Tanaka A, Terashima M, Troels T, Uemura S, Ughi GJ, van Beusekom HM, van der Steen AF, Van Es GA, van Soest G, Virmani R, Waxman S, Weissman NJ, Weisz G; International Working Group for Intravascular Optical Coherence Tomography (IWG-IVOCT). Consensus standards for acquisition, measurement, and reporting of intravascular optical coherence tomography studies: a report from the International Working Group for Intravascular Optical Coherence Tomography Standardization and Validation. *J Am Coll Cardiol*. 2012;59:1058-72.

10. Prati F, Cera M, Ramazzotti V, Imola F, Giudice R, Albertucci M. Safety and feasibility of a new non-occlusive technique for facilitated intracoronary optical coherence tomography (OCT) acquisition in various clinical and anatomical scenarios. *EuroIntervention*. 2007;3:365-70.

11. Gutiérrez-Chico JL, Cortés C, Schincariol M, Jaguszewski M. A formula to calculate the contrast volume required for optimal imaging quality in optical coherence tomography with non-occlusive technique. *Cardiol J*. 2018;25:574-81.

12. Prabhu S, Schikorr T, Mahmoud T, Jacobs J, Potgieter A, Simonton C. Engineering assessment of the longitudinal compression behaviour of contemporary coronary stents. *EuroIntervention*. 2012;8:275-81.

13. Tomberli B, Mattesini A, Baldereschi GI, Di Mario C. A Brief History of Coronary Artery Stents. *Rev Esp Cardiol (Engl Ed)*. 2018;71:312-9.

14. Barkholt TO, Webber B, Holm NR, Ormiston JA. Mechanical properties of the drug-eluting bioresorbable magnesium scaffold compared with polymeric scaffolds and a permanent metallic drug-eluting stent. *Catheter Cardiovasc Interv*. 2020;96:E674-82.

15. Silber S, Gutiérrez-Chico JL, Behrens S, Witznitchler B, Wiemer M, Hoffmann S, Slagboom T, Harald D, Suryapranata H, Nienaber C, Chevalier B, Serruys PW. Effect of paclitaxel elution from reservoirs with bioabsorbable polymer compared to a bare metal stent for the elective percutaneous treatment of de novo coronary stenosis: the EUROSTAR-II randomised clinical trial. *EuroIntervention*. 2011;7:64-73.

16. Virmani R, Guagliumi G, Farb A, Musumeci G, Grieco N, Motta T, Mihalesic L, Tespili M, Valsecchi O, Kolodgie FD. Localized hypersensitivity and late coronary thrombosis secondary to a sirolimus-eluting stent: should we be cautious? *Circulation*. 2004;109:701-5.

17. Gutiérrez-Chico JL, Jaguszewski M, Comesana-Hermo M, Correa-Duarte MA, Martinis-Pardo L, Hermida-Prieto M. Macrophagic enhancement in optical coherence tomography imaging by means of superparamagnetic iron oxide nanoparticles. *Cardiol J*. 2017;24:459-66.

18. Wu P, Gutiérrez-Chico JL, Tauzin H, Yang W, Li Y, Yu W, Chu M, Guillon B, Bai J, Meneveau N, Wijns W, Tu S. Automatic stent reconstruction in optical coherence tomography based on a deep convolutional model. *Biomed Opt Express*. 2020;11:3374-94.

Supplementary data

Supplementary Table 1. Definition of the different stent patterns.

Supplementary Table 2. Summary of the technical requirements for each step of the protocol.

The supplementary data are published online at:

<https://eurointervention.pronline.com/doi/10.4244/EIJ-D-20-00598>



Supplementary data

Supplementary Table 1. Definition of the different stent patterns.

| Stent platform | Sinusoidal hoops | Longitudinal connector | Model and OCT |
|---------------------------------------|--|--|-------------------|
| MULTI-LINK RX ULTRA | In-phase | <ul style="list-style-type: none"> • Peak-to-peak • Straight • Linking 2 adjacent hoops | Figure 3, panel A |
| MULTI-LINK RX PIXEL | In-phase | <ul style="list-style-type: none"> • Peak-to-peak • Straight • Linking 3 consecutive hoops, alternating with connectors linking only 2 adjacent hoops | Figure 3, panel B |
| MULTI-LINK PENTA/ZETA | In-phase | <ul style="list-style-type: none"> • Peak-to-peak • Sinusoidal ACCESS connectors, consisting of 5 turns (2 peaks at each side of the connector) | Figure 3, panel C |
| MULTI-LINK 8/VISION platform (XIENCE) | In-phase | <ul style="list-style-type: none"> • Peak-to-peak • Typical crenelated shape | Figure 3, panel D |
| Firebird/Firehawk | In-phase | <ul style="list-style-type: none"> • Valley-to valley or peak-to-peak (one design or the other) • S-shaped connector at the obtuse angle (3 turns, one peak at each side of the connector) • Last hoop at proximal and distal extremes are connected by peak-to-valley S-shaped connector | Figure 3, panel E |
| BiodivYsio | In-phase | <ul style="list-style-type: none"> • Peak-to-peak, alternating with valley-to-valley in the adjacent rings • S-shaped connector at the inferior peak or upper valley (3 turns, one peak at each side of the connector) | Figure 3, panel F |
| Express platform (TAXUS) | Sinusoidal hoops, alternating different frequencies (wide hoops with long struts and few peaks, narrow hoops with short struts and more peaks), thus appearing as in-phase or out-of-phase at different points | <ul style="list-style-type: none"> • Peak-to-peak, alternating with valley-to-valley in the adjacent rings | Figure 3, panel G |
| Liberté platform (TAXUS) | In-phase, with asymmetrical and tilted peaks/valleys, giving a typical interdigitated appearance | <ul style="list-style-type: none"> • Direct peak-to-valley connection, possibly due to the asymmetry and tilt of the design | Figure 3, panel H |

| | | | |
|---|--|--|-------------------|
| | | | |
| Element platform (TAXUS/PROMUS/SYNERGY) | Offset (almost out-of-phase) | <ul style="list-style-type: none"> • Peak-to-valley • Short straight connector, aligned with the direction of the slope | Figure 3, panel I |
| Bx Velocity platform (CYPHER) | Out-of-phase | <ul style="list-style-type: none"> • Sinusoidal longitudinal connector • Connecting the slopes (almost peak-to-valley) | Figure 3, panel J |
| Juno platform (BioMatrix) | Out-of-phase | <ul style="list-style-type: none"> • Peak-to-valley • S-shaped connector | Figure 3, panel K |
| PRO-Kinetic platform (Orsiro) | Offset | <ul style="list-style-type: none"> • Mid points of the slopes • Semi-straight connector • From upslope to upslope • Perpendicular to the slopes | Figure 3, panel L |
| Magmaris | Offset | <ul style="list-style-type: none"> • Mid points of the slopes • Sinusoidal connector • From upslope to upslope • Parallel to the slopes | Figure 3, panel M |
| Coroflex | Offset | <ul style="list-style-type: none"> • Mid points of the slopes • Typical step-shaped connector • From downslope to upslope (Coroflex blue) or slopes of the same kind (Coroflex ISAR NEO). | Figure 3, panel N |
| AVE platform (Driver, Endeavor, Resolute) | Out-of-phase | <ul style="list-style-type: none"> • Direct peak-to-valley connection • By welds • Regular structure | Figure 3, panel O |
| Integrity and Onyx platforms (Resolute) | Out-of-phase Irregular alignment (single wire) | <ul style="list-style-type: none"> • Direct peak-to-valley connection • By welds • Connection every 4 peaks • Irregular structure | Figure 3, panel P |
| Nobori | Out-of-phase Regular alignment | <ul style="list-style-type: none"> • Direct peak-to-valley connection • By welds • Connection every 3 peaks • Regular structure | Figure 3, panel Q |
| CoStar | Out-of-phase Typical strut appearance with wells along the struts | <ul style="list-style-type: none"> • Peak-to-valley • Sinusoidal connector with wells | Figure 3, panel R |
| ALEX PLUS | In-phase | <ul style="list-style-type: none"> • Peak-to-slope, alternating with valley-to-slope in the adjacent rings | Figure 3, panel S |
| BiOSS LIM C | In-phase Two differentiated segments linked by 2 longitudinal connectors | <ul style="list-style-type: none"> • Peak-to-slope | Figure 3, panel T |

Supplementary Table 2. Summary of the technical requirements for each step of the protocol.

| Step | Dimensions | ASD | Post-processing |
|----------------------|-------------------|------------|------------------------|
| 1. 3D + ASD | 3D | Yes | Yes |
| 2. 3D tissue view | 3D | No | No |
| 3. Longitudinal view | 2D | Yes | No |
| 4. Stent only | 3D | Yes | Yes |

ASD: automatic strut detection